Petroleum Science 23 (2026) 882–896

Contents lists available at ScienceDirect

Petroleum Science

journal homepage: www.keaipublishing.com/en/journals/petroleum-science

Original Paper

Mechanistic insights into amine-oxide-modified silica nanoparticle-stabilized Pickering emulsions for enhanced heavy oil recovery in heterogeneous reservoirs

Hai-Hua Pei [a,b,c,*], Jian-Wei Zhao [a,b,c], Yang Liu [a,b,c], Jian Zhang [a,b,c], Gui-Cai Zhang [a,b,c]

[a] State Key Laboratory of Deep Oil and Gas, China University of Petroleum (East China), Qingdao, 266580, Shandong, China
[b] School of Petroleum Engineering, China University of Petroleum (East China), Qingdao, 266580, Shandong, China
[c] Shandong Key Laboratory of Oil and Gas Field Chemistry, China University of Petroleum (East China), Qingdao, 266580, Shandong, China

ARTICLE INFO

Article history:
Received 7 June 2025
Received in revised form
3 November 2025
Accepted 4 November 2025
Available online 10 November 2025

Edited by Yan-Hua Sun

Keywords:
Pickering emulsion
Surface-modified nanoparticles
Mobility control
Pore-scale mechanisms
Enhanced heavy oil recovery

ABSTRACT

To address the critical stability and mobility control limitations of conventional surfactant-stabilized emulsions, this study introduces a novel Pickering emulsion system stabilized by lauramidopropyl-amine oxide (LAO)-modified SiO_2 nanoparticles for enhanced heavy oil recovery. An aromatic hydrocarbon mixture was used as the oil phase, and the emulsion formulation (0.05 wt% LAO, pH 7.0) was systematically optimized through stability evaluations and rheological analyses. The optimized emulsion exhibited high stability, reversible shear-thinning behavior (> 90% viscosity recovery post-shearing), and predominantly elastic viscoelastic characteristics ($G'/G'' > 10$), which are attributed to the rigid interfacial film formed by LAO-modified SiO_2 nanoparticles. Core flooding tests demonstrated exceptional plugging performance (resistance coefficient, $F_R = 124.3$; residual resistance coefficient, $F_{RR} = 24.1$) and achieved 29.6% incremental oil recovery—significantly exceeding conventional surfactant-stabilized emulsions (11.1%). A heterogeneous dual-core flooding experiment (permeability contrast = 5:1) confirmed superior conformance control with 33.6% tertiary oil recovery. Microscopic visualization revealed three synergistic mechanisms: (1) viscosity reduction and emulsification for enhanced heavy oil mobility; (2) flow diversion via Jamin effect-induced pore-throat blockage; and (3) pore-scale viscoelastic mobilization of residual oil. These mechanisms collectively enhanced macroscopic sweep efficiency and microscopic displacement efficiency, substantially improving heavy oil recovery in heterogeneous reservoirs. This work provides fundamental insights into Pickering emulsion transport in porous media and establishes a practical strategy for enhanced heavy oil recovery in heterogeneous reservoirs.

1. Introduction

Heavy oil, representing over 30% of global hydrocarbon resources, has become a critical unconventional energy source due to the depletion of conventional light oil reserves (Gomaa et al., 2024; Malozyomov et al., 2023; Seidy-Esfahlan et al., 2024). However, its extraction poses significant challenges due to its high viscosity (> 100 mPa·s) and low mobility, resulting in recovery factors typically below 30% (Liu et al., 2020; Sun et al., 2024; Yao et al., 2023). In thin or deep heavy oil reservoirs, where thermal methods are often infeasible, waterflooding is commonly employed but proves ineffective due to severe viscous fingering and limited sweep efficiency caused by unfavorable water–oil mobility ratios (Dong et al., 2019; Li et al., 2023; Kargozarfard et al., 2019; Wang et al., 2021). Therefore, improving oil recovery in these waterflooded heavy oil reservoirs remains a substantial technical challenge.

Emulsion flooding has emerged as a promising enhanced oil recovery (EOR) technique for waterflooded reservoirs (Ahmadi and Chen, 2020; Li et al., 2024; Mahboob et al., 2022; Mariyate and Bera, 2021, 2022; Zhou et al., 2019). For instance, Sarma et al. (1998) conducted comparative core flooding experiments evaluating water, solvent, and emulsion flooding for heavy oil recovery (2830 mPa·s). Their results demonstrated that emulsion flooding

* Corresponding author.
E-mail address: peihaihua@upc.edu.cn (H.-H. Pei).
Peer review under the responsibility of China University of Petroleum (Beijing).

https://doi.org/10.1016/j.petsci.2025.11.012

with 30% condensate content improved recovery by up to 80% compared to solvent flooding and achieved 2–3 times higher recovery than water flooding, highlighting its superiority for heavy oil production. Similarly, Karambeigi et al. (2015) developed a diesel-based emulsion system stabilized with sodium dodecyl sulfate (SDS). Their sandpack flooding experiments achieved an incremental oil recovery of 28% following injection of a 0.25 PV (pore volume) emulsion slug. Despite these advances, surfactant-stabilized emulsions face limitations in reservoir conditions, including reduced stability due to surfactant adsorption onto rock surfaces (Kumar and Mandal, 2018; Salehnia et al., 2025). Furthermore, they often exhibit insufficient thermal and chemical stability, leading to emulsion breakdown, droplet coalescence, and compromised mobility control (Ahmadi et al., 2019).

Pickering emulsions stabilized by solid nanoparticles demonstrate superior stability and tunable rheological properties compared to conventional surfactant-based systems (Adil and Onaizi, 2022; Liu et al., 2021; Nourafkan et al., 2019; Santos et al., 2023). Silica nanoparticles are widely used in EOR applications due to their nanoscale size, cost-effectiveness, and excellent compatibility with sandstone reservoirs (Duodu and Ju, 2025; Jia and Kang, 2025; Liang et al., 2022). Maurya and Mandal (2018) demonstrated synergistic stabilization of oil-in-water (O/W) emulsions using silica nanoparticles and ionic surfactants (SDS and CTAB), observing superior performance with CTAB attributed to favorable electrostatic interactions with the silica surface. Similarly, Pei et al. (2018) achieved over 40% post-waterflood recovery for viscous heavy oil (325 mPa·s) by utilizing CTAB with hydrophilic silica nanoparticles. Singh et al. (2025) developed SiO_2/olefin sulfonate microemulsions, which achieved 29% recovery through combined electrostatic and steric stabilization, representing a 45% improvement over conventional surfactant systems (20%). Most notably, Qin et al. (2020) demonstrated the effectiveness of *in situ* synthesized silica nanoparticles for microemulsion stabilization in heterogeneous Arkose sandstone reservoirs. Their nanoparticle-stabilized microemulsions yielded 34.3% incremental oil recovery after waterflooding, surpassing surfactant-only systems by 14.3%. These results collectively underscore the significant potential of Pickering emulsions as high-performance EOR agents, particularly in heterogeneous reservoirs exhibiting adverse mobility conditions.

While the formulation of nanoparticle-stabilized emulsions has been extensively studied (Heidari-Dalfard et al., 2024), the fundamental mechanisms governing their performance—particularly the relative contributions of interfacial viscoelasticity and droplet jamming to sweep efficiency enhancement—remain poorly understood. This study aims to bridge this knowledge gap by developing a novel Pickering emulsion system stabilized by amine oxide-modified silica nanoparticles and systematically investigating its heavy oil recovery mechanisms. Specifically focusing on the distinct roles of interfacial viscoelasticity, droplet aggregation, and the Jamin effect in enhancing sweep efficiency and mobility control, we employ an integrated approach combining rheological characterization, parallel dual-core flooding experiments, and microscopic visualization. This work provides a quantitative analysis of the system's heavy oil recovery enhancement in heterogeneous reservoirs, offering novel mechanistic insights for designing advanced emulsion-based EOR strategies.

2. Experimental materials and methods

2.1. Experimental materials

Laurylamidopropylamine oxide (LAO), an amphoteric surfactant (30 wt% active content), was supplied by Linyi Lvsen Chemical Co. (Shandong, China). Hydrophilic SiO_2 nanoparticles (median diameter: 12 nm) were purchased from Sigma-Aldrich. The heavy oil sample, obtained from the CZ reservoir in the Shengli Oilfield, had a viscosity of 3865 mPa·s at 70 °C. The physicochemical properties of the heavy oil are detailed in Table 1. The oil phase for emulsion preparation was an aromatic hydrocarbon mixture (toluene/xylene = 1:2 (v/v)). As shown in Fig. 1, the viscosity of CZ heavy oil decreased significantly with aromatic solvent concentration, achieving > 70% reduction at 5 wt% solvent and > 90% at 10 wt%. This significant viscosity reduction demonstrates the mixture's exceptional viscosity-reducing capability through colloidal dispersion and solvation effects, which are critical for improving heavy oil mobility. All experimental solutions were prepared using synthetic formation brine, with the ionic composition detailed in Table 2.

2.2. Preparation and characterization of Pickering emulsions

The Pickering emulsions were prepared by dispersing SiO_2 nanoparticles (1.0 wt%) and varying concentrations of the amphoteric surfactant LAO in synthetic formation brine (pH = 7.0). The resulting aqueous suspension was mixed with the aromatic solvent mixture (toluene/xylene = 1:2 (v/v)) at a fixed oil-to-water volume ratio of 1:1 and homogenized with an Ultra-Turrax (IKA, Germany) at 10,000 rpm for 5 min to form stable emulsions. For morphological characterization, emulsion samples were collected using a precision dropper and immediately analyzed using a CX33 optical microscope (Olympus, Japan) to evaluate droplet morphology. Droplet size distribution was quantified via laser diffraction (Mastersizer 3000, Malvern Panalytical). For fluorescence characterization, rhodamine B-labeled (10^{-3} mol/L) silica nanoparticles were incorporated into emulsions and their spatial distribution was visualized by confocal laser scanning microscopy (CLSM).

2.3. Stability evaluation of Pickering emulsions

Emulsion stability was evaluated using a multiple light scattering analyzer (TURBISCAN Lab Expert, France) at 70 °C. The instrument quantifies variations in backscattered light intensity (ΔBS) from incident beams interacting with droplets. Backscattering profiles were generated from the correlation between backscattered and incident light intensities. The Turbiscan stability index (TSI) was calculated as follows:

$$\mathrm{TSI} = \sqrt{\frac{\sum_{i=1}^{n} (x_i - x_{BS})^2}{n-1}} \quad (1)$$

where x_i is the scan-specific mean backscattered light intensity; x_{BS} is the overall mean intensity; and n is the total number of scans. Lower TSI values indicate superior emulsion stability over time.

2.4. Rheological behavior of Pickering emulsions

The rheological behavior of the Pickering emulsion was systematically characterized using an MCR92 rheometer (Anton Paar) equipped with a CC-39 rotor at 70 °C. Steady-state shear measurements were first performed across a wide shear rate range (10^{-3} to 10^{3} s^{-1}) to establish the baseline flow properties. Subsequently, a three-stage shear recovery test was conducted, beginning with a low shear rate (1 s^{-1} for 5 min), followed by high shear conditions (100 s^{-1} for 15 min), and returning to low shear (1 s^{-1} for 5 min) to evaluate the emulsion's structural recovery. The

Table 1
Basic properties of CZ heavy oil.

Viscosity at 70 °C, mPa·s	Density at 70 °C, g/cm^3	SARA analysis, wt%			
		Saturates	Aromatics	Resins	*n*-Heptane asphaltenes
3865	0.98	32.97	26.09	33.85	7.09

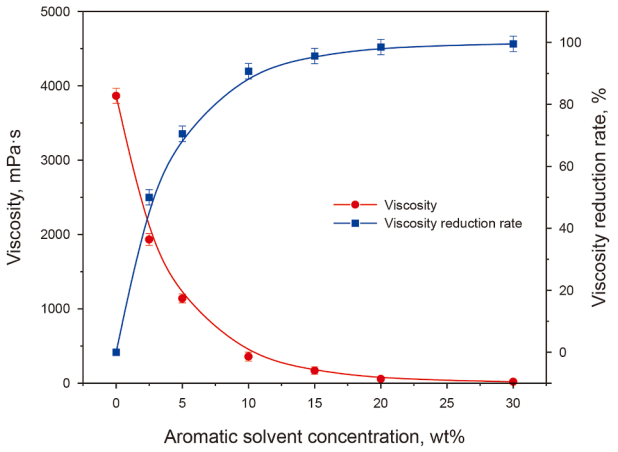

Fig. 1. Viscosity reduction of heavy oil as a function of aromatic solvent concentration.

Table 2
Ionic composition of synthetic formation brine.

Ion content, mg·L^{-1}						Total salinity, mg·L^{-1}
$K^+ + Na^+$	Ca^{2+}	Mg^{2+}	SO_4^{2-}	HCO_3^-	Cl^-	
3982	221	125	48	496	6573	11445

viscosity recovery behavior was quantified using two key parameters, the initial recovery rate (R_1) and final recovery rate (R_2), calculated as follows:

$$R_1 = \mu_1 / \mu_0 \times 100\% \quad (2)$$

$$R_2 = \mu_2 / \mu_0 \times 100\% \quad (3)$$

where μ_0 is the resting viscosity, mPa·s; μ_1 is the initial recovery viscosity, mPa·s; and μ_2 is the final recovery viscosity, mPa·s.

Dynamic rheological characterization was then performed through sequential stress and frequency sweeps. The linear viscoelastic range was first determined via stress sweep measurements, followed by frequency-dependent viscoelastic property evaluation across an angular frequency range of 0.1–100 rad/s.

2.5. Plugging performance evaluation of Pickering emulsions

Core flooding experiments were performed at reservoir conditions (70 °C) to evaluate the plugging performance of Pickering emulsions. Homogeneous artificial sandstone cores (10 cm length × 2.5 cm diameter) were utilized, exhibiting an average permeability of 1500±50 mD. Prior to testing, cores were chemically treated to maintain hydrophilic wettability (contact angle = 30°±5°), representing the water-wet characteristics of typical sandstone reservoirs. The experimental procedure comprised three sequential stages: (1) Initial waterflooding: Synthetic brine was injected at 0.1 mL/min until the pressure stabilized at ΔP_A, establishing the baseline. (2) Emulsion flooding: Pickering emulsion was injected at 0.1 mL/min until the pressure stabilized at ΔP_E. (3) Post-emulsion waterflooding: Brine was reinjected at 0.1 mL/min until the pressure stabilized at ΔP_B. Plugging performance was quantified using the resistance coefficient (F_R) and residual resistance coefficient (F_{RR}), defined as follows:

$$F_R = \Delta P_E / \Delta P_A \quad (4)$$

$$F_{RR} = \Delta P_B / \Delta P_A \quad (5)$$

where F_R represents the dimensionless resistance coefficient; F_{RR} denotes the dimensionless residual resistance coefficient; ΔP_A is the stabilized pressure during initial waterflooding, kPa; ΔP_E corresponds to the stabilized pressure during emulsion flooding, kPa; and ΔP_B indicates the stabilized pressure during post-emulsion waterflooding, kPa.

2.6. Core flooding experiments

Core flooding experiments were conducted at reservoir temperature (70 °C) to assess the enhanced oil recovery performance of Pickering emulsions in single-core and dual-core systems. Single-core tests used homogeneous artificial sandstone cores (10 cm length × 2.5 cm diameter) and an average permeability of 1500±50 mD. Dual-core tests employed matched core pairs (identical dimensions) with permeability contrasts of 3:1 and 5:1, simulating moderate-to-high reservoir heterogeneity. All cores were preconditioned to maintain hydrophilic wettability (contact angle = 30°±5°), representing typical water-wet sandstone reservoirs. The dual-core apparatus is shown in Fig. 2. The experimental procedure comprised four stages: (1) Oil saturation was established by injecting crude oil at 0.1 mL/min until full saturation was achieved. (2) Initial waterflooding was conducted at 0.1 mL/min while continuously monitoring effluent oil–water volumes until the water cut exceeded 98%. (3) A 0.5 PV slug of emulsion was injected at 0.1 mL/min (4) Subsequent waterflooding was performed at the same injection rate until no additional oil production was observed. Fluid production and differential pressure across both cores were monitored to evaluate emulsion performance in heterogeneous systems.

2.7. Microscopic visualization experiments

The pore-scale displacement mechanisms of Pickering emulsion flooding were studied using a specially designed glass-etched

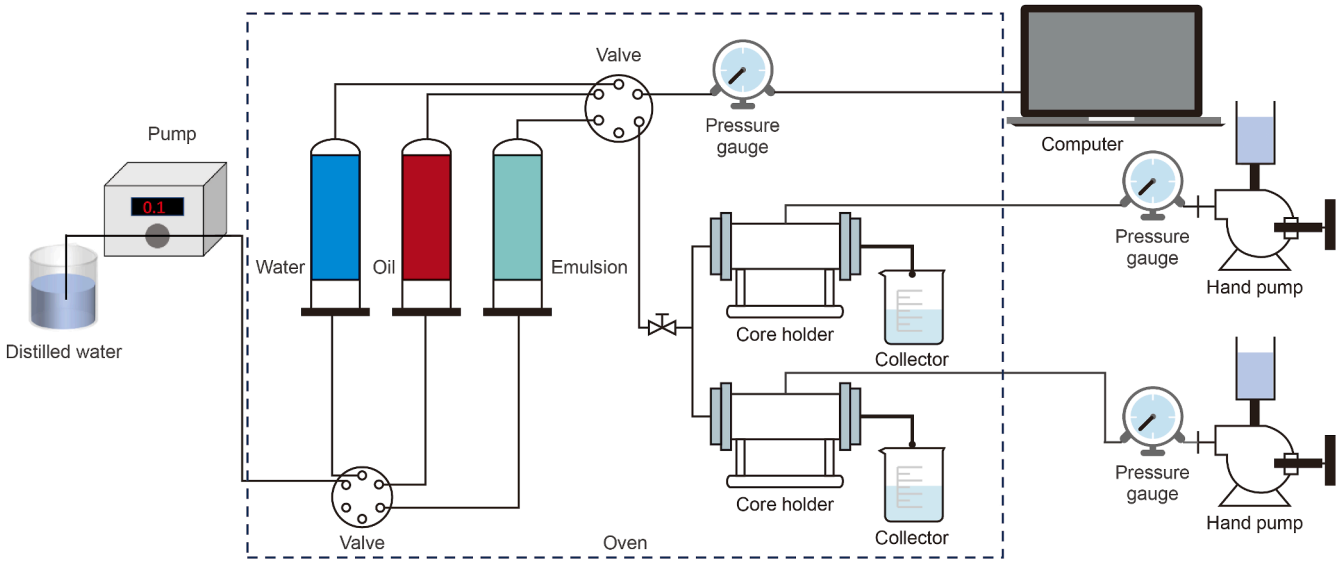

Fig. 2. Schematic diagram of the dual-core flooding experimental setup.

micromodel (35 mm × 35 mm × 6 mm), replicating the pore-throat architecture of a heavy oil reservoir. The micromodel featured a representative bimodal pore-size distribution (macropores: 60±5 μm; micropores: 10±2 μm) and a hydrophilic surface (contact angle = 30°±5°), reproducing the pore geometry and wettability characteristics of heavy-oil-bearing sandstones. The experimental setup is illustrated in Fig. 3. The micromodel was evacuated and saturated sequentially with water and crude oil at 0.001 mL/min using a high-accuracy syringe pump. The experimental procedure comprised two stages: an initial waterflooding at 0.001 mL/min until water breakthrough, followed by continuous Pickering emulsion injection at the same rate until oil production ceased. *In situ* pore-scale displacement dynamics were captured using a high-resolution imaging system for subsequent analysis of emulsion transport and oil mobilization mechanisms within the porous network.

3. Results and discussion

3.1. Preparation and characterization of Pickering emulsions

3.1.1. Optimization of Pickering emulsions

The inherent hydrophilicity and limited interfacial adsorption capacity of SiO_2 nanoparticles require surface modification for effective emulsion stabilization. Laurylamidopropylamine oxide (LAO), as an amphoteric surfactant, exhibits cationic characteristics below its isoelectric point (pI = 9.4), which facilitates hydrophobic modification of nano-SiO_2 surfaces through electrostatic adsorption (Zhang et al., 2018). At pH 7, LAO molecules adopt a protonated cationic state through the protonation of their amine groups, enabling strong interfacial adhesion via electrostatic interactions between the cationic LAO and the negatively charged silanol moieties on the nano-SiO_2 surface. This LAO-induced

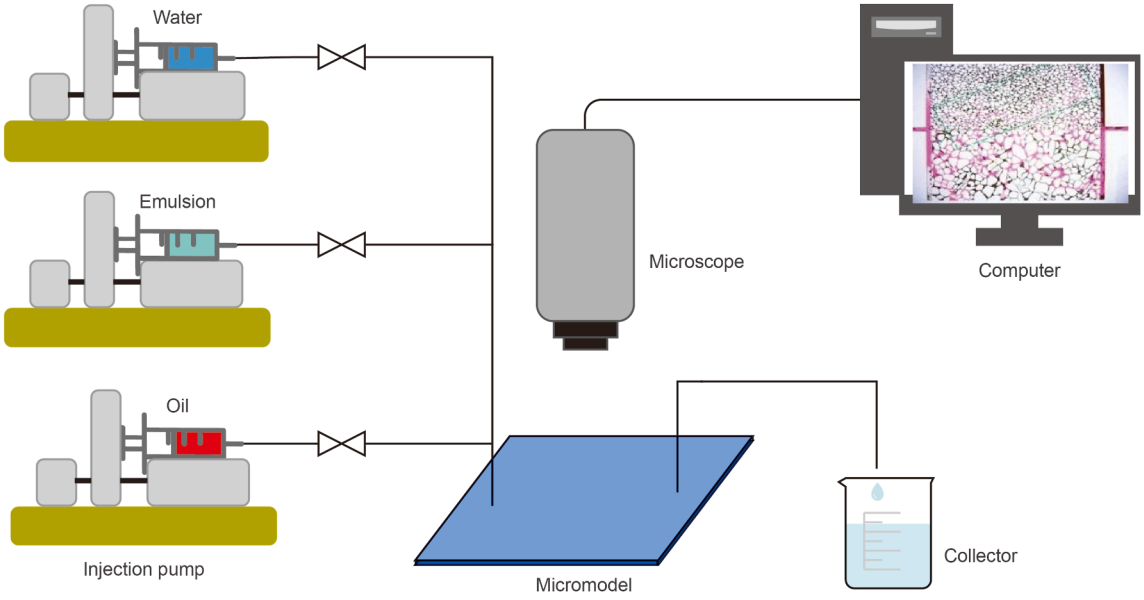

Fig. 3. Schematic diagram of the microscopic visualization experimental setup.

surface modification reduces nanoparticle hydrophilicity and enhances interfacial activity, allowing the modified nano-SiO_2 particles to stabilize emulsions more effectively (Binks et al., 2007).

The optimization process was systematically evaluated using 1.0 wt% nano-SiO_2 modified with LAO concentrations ranging from 0.01 to 0.10 wt% at pH 7.0. Emulsion stability was quantified using Turbiscan stability analysis (TSI), where lower TSI values indicate greater stability. Fig. 4 presents the TSI curves of the Pickering emulsion stabilized by 1.0 wt% nano-SiO_2 modified with varying LAO concentrations. As shown in Fig. 4, the TSI value initially decreased and then increased with rising LAO concentration, reaching a minimum between 0.03 and 0.05 wt%, corresponding to optimal stability. At LAO concentrations below 0.05 wt%, increasing LAO content reduced TSI values. This enhancement was attributed to LAO-mediated surface modification of the nano-SiO_2, which improved their adsorption at the oil–water interface and promoted denser interfacial film formation. Conversely, when the LAO concentration exceeded 0.05 wt%, the TSI value increased significantly. This destabilization occurred because excessive LAO adsorption over-hydrophobized the nanoparticles, reducing their interfacial affinity and thereby compromising emulsion stability.

3.1.2. Droplet size of Pickering emulsions

Optical microscopy analysis demonstrated that droplet morphology in Pickering emulsions stabilized by 1.0 wt% nano-SiO_2 critically depended on LAO concentration (0.01–0.10 wt%). As shown in Fig. 5, the emulsion droplet size initially decreased and then increased with rising LAO concentration, accompanied by a narrowing and subsequent broadening of the size distribution. The smallest and most uniform droplets occurred at 0.03 wt% LAO. At 0.01 wt% LAO, larger droplets formed due to inadequate nanoparticle modification and insufficient interfacial coverage. Increasing the LAO concentration to 0.03 wt% enhanced nanoparticle adsorption at the oil–water interface, leading to the formation of smaller droplets with a narrower size distribution. Conversely, when the LAO concentration exceeded 0.05 wt%, droplet size increased correspondingly due to excessive LAO adsorption on the nano-SiO_2 particles, which neutralized electrostatic repulsion and induced flocculation. At 0.10 wt% LAO, the droplet size distribution broadened significantly because excess LAO enhanced nanoparticle lipophilicity, promoting droplet coalescence. These results indicate that Pickering emulsions stabilized by LAO-modified nano-SiO_2 particles reach optimal stability at 0.03–0.05 wt% LAO and pH 7, with droplet sizes predominantly ranging from 1 to 10 μm.

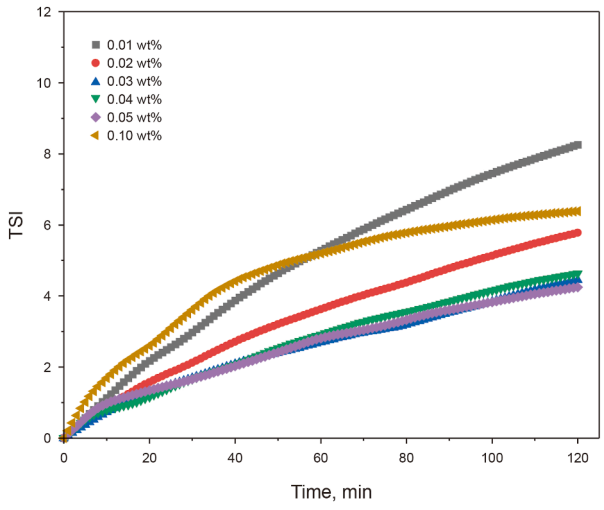

Fig. 4. Turbiscan stability analysis (TSI) curves of Pickering emulsions stabilized by 1.0 wt% nano-SiO_2 modified with varying LAO concentrations.

3.1.3. Stability mechanisms of Pickering emulsions

The stabilization mechanisms of Pickering emulsions are illustrated in Fig. 6. As shown in Fig. 6(a), LAO molecules exist in a protonated cationic state at pH 7 due to the protonation of their amine groups. This molecular configuration facilitates strong interfacial adhesion through electrostatic interactions between the cationic LAO and negatively charged SiO_2 nanoparticles. The hydrophobic lauryl chains of LAO extend outward, enhancing the nanoparticle hydrophobicity and promoting their effective adsorption at the oil–water interface. The dense aggregation of nanoparticles at the interface forms a solid-like barrier that inhibits droplet coalescence, enhancing the emulsion's stability (Worthen et al., 2014). Fig. 6(b) provides visual confirmation of LAO-modified SiO_2 nanoparticle adsorption via confocal laser scanning microscopy (CLSM). The observed fluorescence intensity demonstrates the formation of a densely packed nanoparticle film at the oil–water interface. This nanostructured film significantly increases interfacial rigidity, which is a critical factor for the stability of Pickering emulsions (Chevalier and Bolzinger, 2013). Collectively, these synergistic mechanisms ensure long-term emulsion stability under reservoir conditions.

3.2. Rheological behavior of Pickering emulsions

3.2.1. Bulk viscosity of Pickering emulsions

Stable Pickering emulsions with minimal droplet sizes were obtained at LAO concentrations of 0.01–0.05 wt%. Fig. 7 presents the steady-state shear curves of Pickering emulsions stabilized by 1.0 wt% nano-SiO_2 particles modified with different LAO concentrations. The steady-state shear curves exhibited three distinct regions: (1) a zero-shear plateau ($< 0.01\ s^{-1}$), characterized by constant viscosity, reflecting structural integrity under quiescent conditions; (2) a shear-thinning regime, where viscosity declined due to the disruption of interdroplet bridging networks; and (3) a high-shear Newtonian plateau, where viscosity stabilized with increasing shear rates. Notably, zero-shear viscosity increased with LAO concentration. This viscosity enhancement stems from diminished electrostatic repulsion between nano-SiO_2 particles, which facilitates stronger interdroplet interactions and the formation of an interconnected nanoparticle network within the continuous phase (Benyaya et al., 2024). This elevated zero-shear viscosity enhances mobility control in heterogeneous reservoirs, while the shear-thinning behavior improves injectability. The pseudoplastic behavior originates from the shear-induced, reversible breakdown of the nanoparticle network, with viscosity increasing with LAO concentration. Coupled with the optimal emulsion stability at 0.03–0.05 wt% LAO, these results demonstrate that LAO concentration precisely controls both the microstructure and macroscopic rheological properties of Pickering emulsions.

3.2.2. Shear viscosity recovery of Pickering emulsions

The shear stability of Pickering emulsions under reservoir injection conditions was assessed using three-stage shear-recovery test, alternating between low-shear ($1\ s^{-1}$), high-shear ($100\ s^{-1}$), and recovery ($1\ s^{-1}$) phases. As shown in Fig. 8(a), emulsions stabilized by LAO-modified nano-SiO_2 exhibited pronounced shear-dependent rheological behavior. Under sustained low-shear ($1\ s^{-1}$), viscosity gradually decreased while retaining structural integrity. Conversely, high-shear conditions ($100\ s^{-1}$) induced an immediate viscosity reduction followed by stabilization, indicating substantial disruption of the interdroplet bridging network.

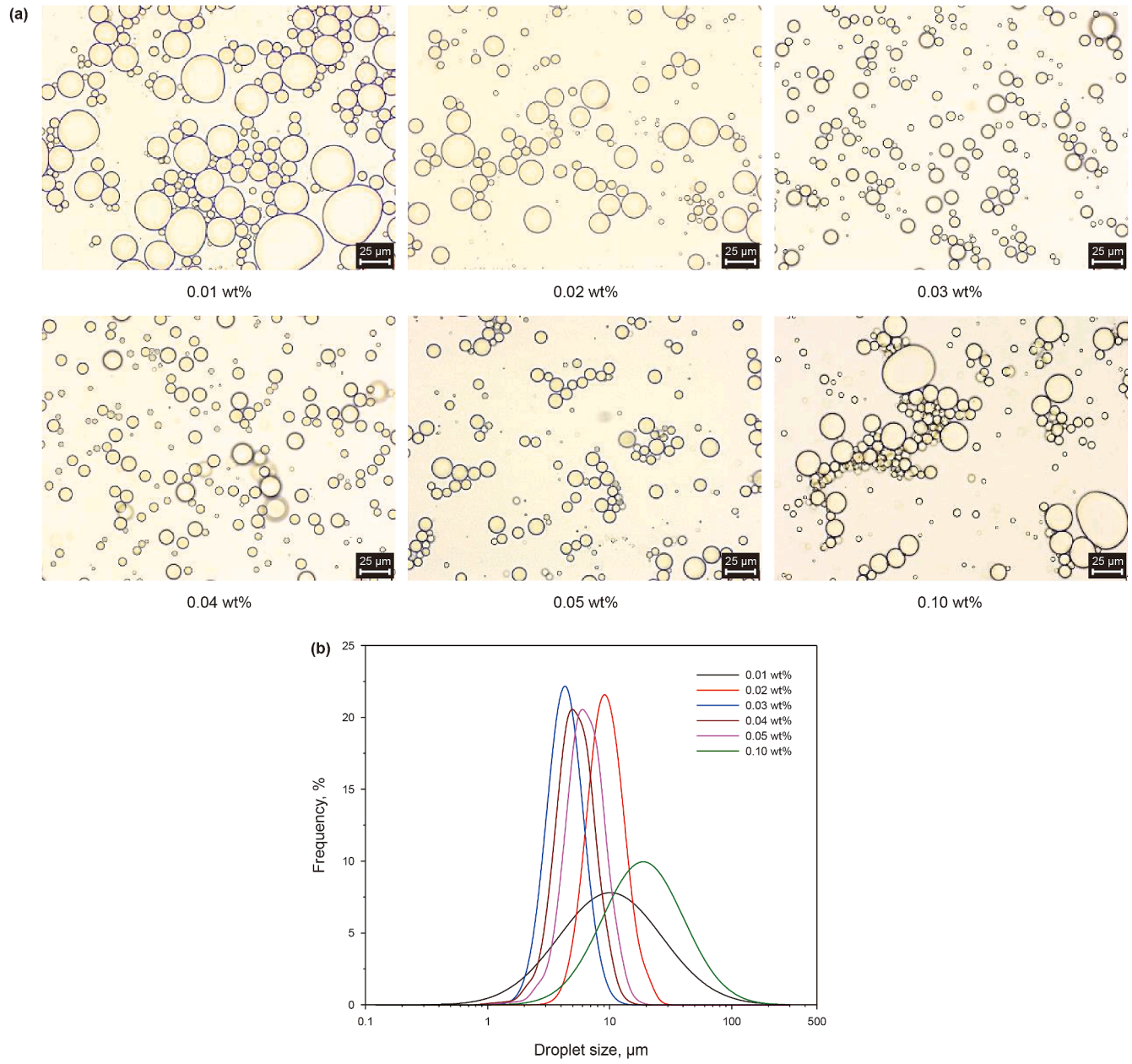

Fig. 5. Characterization of Pickering emulsions stabilized by 1.0 wt% nano-SiO_2 modified with varying LAO concentrations. (**a**) Optical micrographs illustrating emulsion morphology; (**b**) particle size distribution profiles.

During the recovery phase (1 s^{-1}), all systems regained viscosity upon re-exposure to low-shear conditions, though recovery efficiency varied significantly. This behavior indicates that high-shear processes cause partially irreversible microstructural alterations, while sufficient interfacial stability enables partial viscosity restoration (Ding et al., 2022). These reversible shear-thinning properties are advantageous for EOR applications: High-shear viscosity reduction facilitates efficient injection, while partial recovery at reservoir shear rates maintains structural stability and mobility control.

Fig. 8(b) demonstrates that the initial viscosity recovery rate (R_1) exhibits a nonlinear relationship with LAO concentration, peaking at 0.03 wt%. This optimum corresponds to maximum shear resistance, as evidenced by its superior R_1 after continuous shear treatment. Conversely, the final viscosity recovery rate (R_2) increases monotonically with LAO concentration, suggesting enhanced structural regeneration at higher surfactant loadings. Notably, the 0.05 wt% LAO-modified nano-SiO_2 system achieved an R_2 value of 90.2%, demonstrating exceptional recovery. This behavior is attributed to the LAO-mediated reduction in interparticle electrostatic repulsion, which facilitates the reformation of interdroplet bridging networks under low-shear conditions (Kumar et al., 2023). The distinct concentration dependence profiles for R_1 and R_2 indicate different underlying mechanisms governing short-term shear resistance versus long-term structural regeneration. These observations support effective microstructural reconstitution under post-injection reservoir conditions (Fuma and Kawaguchi, 2015). The 0.05 wt% LAO formulation represents a promising candidate, as it optimally balances shear stability and recoverability. These concentration-dependent recovery profiles

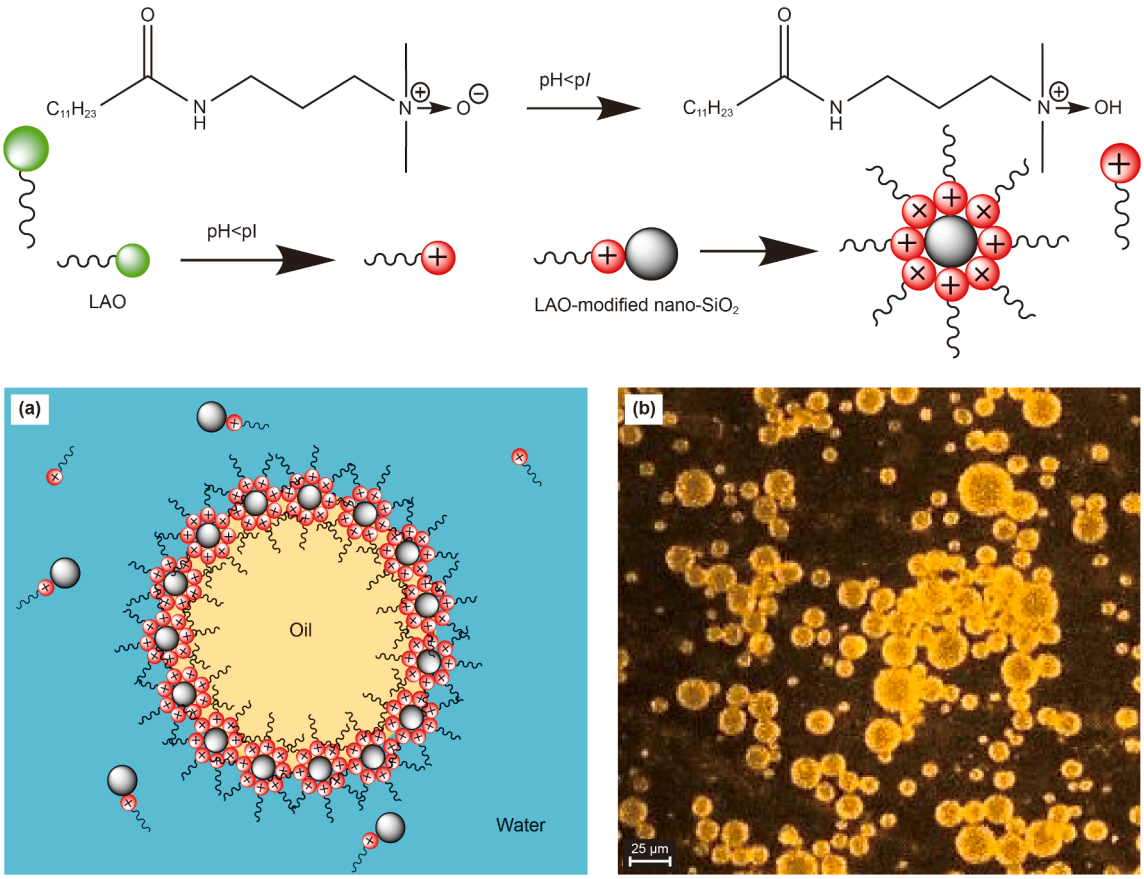

Fig. 6. Stabilization mechanisms of Pickering emulsions stabilized by LAO-modified nano-SiO_2. (**a**) Schematic of LAO-modified nano-SiO_2; (**b**) CLSM image of Pickering emulsions stabilized by 1.0 wt% nano-SiO_2 modified with 0.05 wt% LAO.

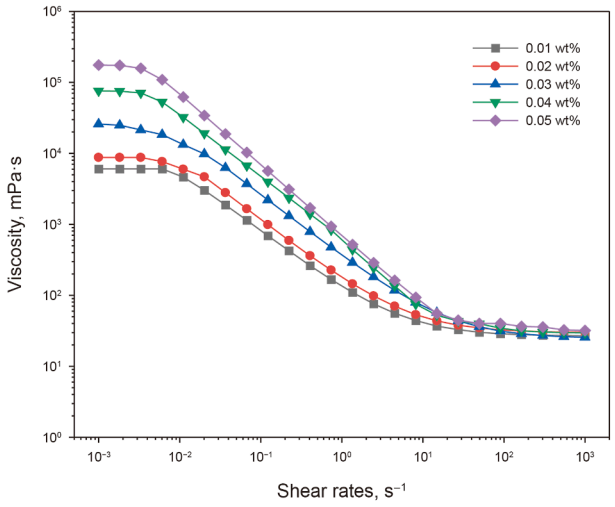

Fig. 7. Steady-state shear curves of Pickering emulsions stabilized by 1.0 wt% nano-SiO_2 modified with different LAO concentrations.

offer valuable insights for designing injectable emulsion systems with tunable rheological properties for subsurface applications.

3.2.3. Dynamic viscoelastic behavior of Pickering emulsions

Frequency sweep tests at a constant strain amplitude of 0.1% were performed to characterize the viscoelastic properties of Pickering emulsions stabilized by LAO-modified nano-SiO_2. Fig. 9 presents the angular frequency (ω) dependence of the storage modulus (G') and loss modulus (G'') for emulsions with LAO concentrations ranging from 0.01 to 0.05 wt%. Both moduli displayed LAO concentration-dependent enhancement, with G' increasing more significantly than G''. The 0.01 wt% LAO system exhibited comparable moduli ($G' \approx G''$), indicating predominantly viscous liquid-like behavior. Conversely, the 0.05 wt% LAO formulation demonstrated strong elastic behavior ($G' > 10G''$), signifying substantial network formation (Chen et al., 2017).

Frequency-dependent analysis revealed distinct structural differences among the emulsions. For systems containing 0.01–0.02 wt% LAO, G' exhibited a significant decrease at high frequencies, indicating a shear-induced breakdown of the interfacial nanoparticle network. Increasing LAO concentration progressively shifted this failure threshold to higher frequencies, demonstrating enhanced structural stability. In contrast, the 0.04–0.05 wt% LAO emulsions maintained nearly constant G' values across the entire frequency range, confirming the formation of a robust, shear-resistant network structure. These results demonstrate that LAO concentration critically governs both the magnitude of the elastic response and the frequency-dependent structural stability. Maximum network strength occurred at 0.04–0.05 wt% LAO, where the system transitioned from viscous-dominant to elastic-dominant behavior. This transition is attributed to improved nanoparticle interfacial packing and strengthened interdroplet interactions at higher LAO concentrations.

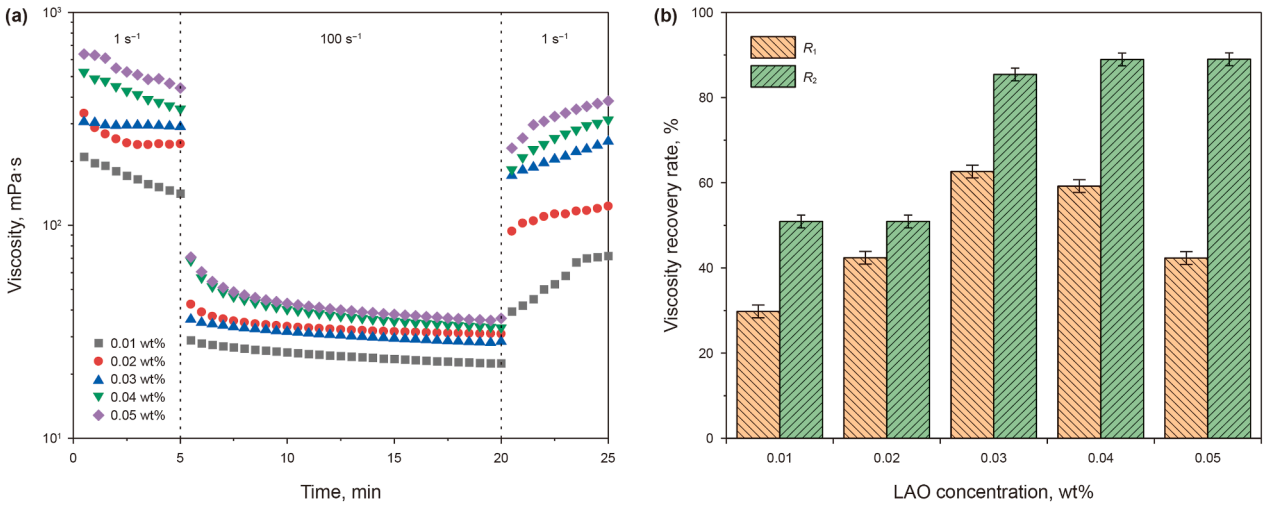

Fig. 8. Viscosity recovery behavior of Pickering emulsions stabilized by 1.0 wt% nano-SiO_2 modified with varying LAO concentrations. (**a**) Viscosity variation; (**b**) viscosity recovery rate.

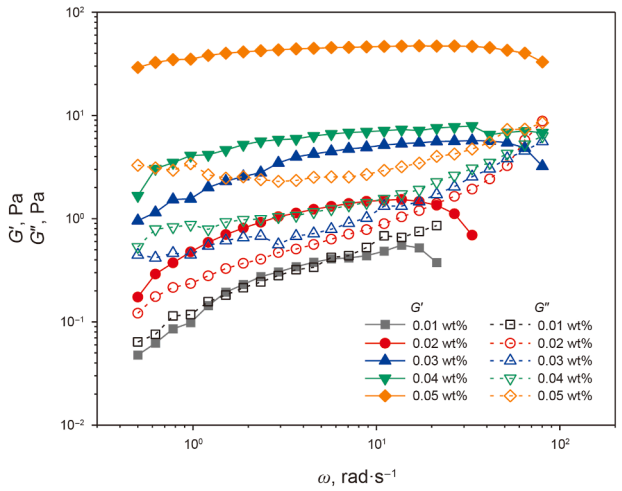

Fig. 9. Storage (G') and loss (G'') moduli versus angular frequency for Pickering emulsions stabilized by 1.0 wt% nano-SiO_2 modified with varying LAO concentrations.

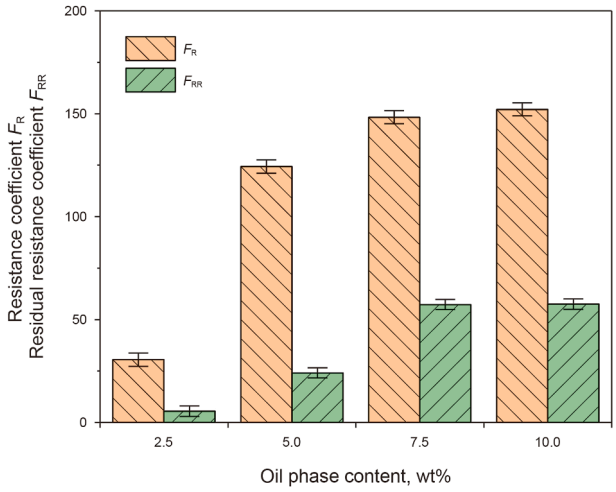

Fig. 10. Resistance coefficients (F_R) and residual resistance coefficients (F_{RR}) for Pickering emulsions with varying oil phase contents.

3.3. Plugging performance of Pickering emulsions

The optimized Pickering emulsion, stabilized by 0.05 wt% LAO-modified nano-SiO_2, demonstrated favorable characteristics: high stability (TSI < 5), a narrow droplet size distribution (1–10 μm), exceptional viscosity recovery (R_2 > 90%), and dominant elastic behavior (G' > 10G''). To systematically evaluate plugging performance, Pickering emulsions were prepared with aromatic solvent concentrations ranging from 2.5 to 10.0 wt%, while maintaining fixed nano-SiO_2 (1.0 wt%) and LAO (0.05 wt%) concentrations. Core flooding experiments (Fig. 10) revealed that plugging efficiency correlated strongly with oil-phase content. Both the resistance coefficient (F_R) and residual resistance coefficient (F_{RR}) increased significantly with increasing oil content up to 5.0 wt%, after which further gains were marginal. Specifically, increasing the oil phase from 2.5 to 5.0 wt% enhanced F_R by 113% (from 58.2 to 124.3) and F_{RR} by 94% (from 12.4 to 24.1), primarily due to an intensified Jamin effect from a higher droplet density. However, incremental improvements diminished substantially above 5.0 wt% oil content, with F_R increasing by only 18% (from 124.3 to 146.8) when the oil phase was increased to 7.5 wt%. This threshold behavior suggests that 5.0 wt% represents the optimal oil content for balancing droplet concentration and flowability in porous media. Below this concentration, insufficient droplet density limits plugging efficiency, whereas higher concentrations may induce droplet coalescence without significantly enhancing blockage (Moradi et al., 2014; Yu et al., 2019). The superior performance of the 5.0 wt% formulation aligns with its optimal droplet dispersion and interfacial nanoparticle packing, as confirmed by microscopy. These results demonstrate that LAO-modified Pickering emulsions attain optimal conformance control at 5.0 wt% oil content, providing effective flow diversion (high F_R) and sustained residual resistance (high F_{RR})—critical for enhanced oil recovery applications.

3.4. Enhanced oil recovery performance of Pickering emulsions

3.4.1. Single-core flooding experiments

Single-core flooding experiments were conducted to evaluate the oil displacement efficiency of Pickering emulsions (5.0 wt% oil phase, stabilized by 1.0 wt% nano-SiO_2 and 0.05 wt% LAO)

compared to surfactant-stabilized emulsions (5.0 wt% oil phase, stabilized by 0.5 wt% LAO) in sandstone cores (1500±50 mD). As shown in Fig. 11(a), the injection of the surfactant-stabilized emulsion produced a transient pressure increase followed by a rapid decline, demonstrating ineffective plugging of waterflooding channels. This response stems from the system's low viscosity and inherent instability, which severely restricts mobility control and limits improvements in sweep efficiency. Consequently, the surfactant-stabilized emulsion achieved only 11.1% additional oil recovery.

In contrast, the Pickering emulsion system demonstrated superior performance, generating significantly higher pressure drop and achieving a substantially higher incremental recovery of 29.6% compared to the LAO surfactant-stabilized emulsion. As shown in Fig. 11(b), a rapid pressure surge occurred upon Pickering emulsion injection, with sustained pressure elevation during subsequent waterflooding. This marked pressure response results from the emulsion's enhanced stability and increased viscosity, which substantially amplify flow resistance via a persistent Jamin effect. Consequently, the Pickering emulsion system provides effective mobility control by diverting subsequent fluid toward unswept zones, leading to a significant improvement in macroscopic sweep efficiency. These results demonstrate the superior performance of Pickering emulsions for enhancing heavy oil recovery in post-waterflood.

3.4.2. Dual-core flooding experiments

Dual-core flooding experiments were conducted at 70 °C to evaluate the enhanced oil recovery performance of Pickering emulsion flooding in heterogeneous reservoirs. The optimized emulsion—formulated with 5.0 wt% oil phase, stabilized by 1.0 wt % nano-SiO_2 and 0.05 wt% LAO—was tested in dual-core setups with permeability contrasts of 3:1 and 5:1. Core parameters and flooding data are summarized in Table 3. As illustrated in Fig. 12, dynamic pressure and flow rate distributions revealed distinct flooding behavior. During initial waterflooding, preferential flow occurred predominantly through the high-permeability cores, with fractional flow ratios disproportionately favoring these pathways (85%–92% for dual-core setups with permeability contrast of 3:1 and 88%–95% for that of 5:1). Upon Pickering emulsion injection, fluid flow was redistributed through a two-stage mechanism: (1) initial infiltration into the high-permeability cores, where elevated viscosity and interfacial viscoelasticity increased flow resistance, followed by (2) progressive diversion into the low-permeability cores via pore-throat blockage induced by the Jamin effect (Su et al., 2021). This increased fractional flow rates in the low-permeability cores by 35%–48% compared to waterflooding, confirming effective plugging of the high-permeability channels and enhanced macroscopic sweep efficiency.

The Pickering emulsion system exhibited permeability-dependent conformance control, with enhanced performance in more heterogeneous formations (Table 3). Tertiary oil recovery increased from 29.8% at a permeability contrast of 3:1 to 33.6% at a contrast of 5:1. This behavior arises from two synergistic mechanisms: (1) Preferential emulsion accumulation in the high-permeability cores creates progressively greater flow resistance with increasing permeability contrast. (2) The resulting pressure differential drives more effective fluid diversion into the low-permeability cores (Demikhova et al., 2016). These findings confirm that the Pickering emulsion provides superior profile control in heterogeneous formations, with performance improvements scaling with permeability variation (Yang et al., 2024). The results underscore the system's exceptional capability to mitigate unbalanced fluid distributions and enhance conformance control under heterogeneous reservoir conditions.

3.5. Microscopic mechanisms of Pickering emulsion flooding

Microscopic visualization experiments were conducted to investigate the mechanisms underlying the enhancement of heavy oil recovery using Pickering emulsions stabilized by LAO-modified nano-SiO_2. The results reveal three dominant displacement mechanisms: (1) viscosity reduction and emulsification for enhanced heavy oil mobility, (2) flow diversion via Jamin-effect-induced pore-throat blockage, and (3) pore-scale viscoelastic mobilization of residual oil.

3.5.1. Viscosity reduction and emulsification for enhanced heavy oil mobility

The LAO-modified SiO_2 nanoparticles were highly effective at stabilizing Pickering emulsions, and the emulsion droplets significantly reduced the viscosity of heavy oil upon interacting with it in the presence of aromatic hydrocarbons. Fig. 13(a) shows rapid mixing upon emulsion–oil contact, evidenced by interfacial penetration and a chromatic transition from red to yellow (Fig. 13 (b)). This visual transformation directly demonstrated a significant reduction in heavy oil viscosity. The miscibility process produced

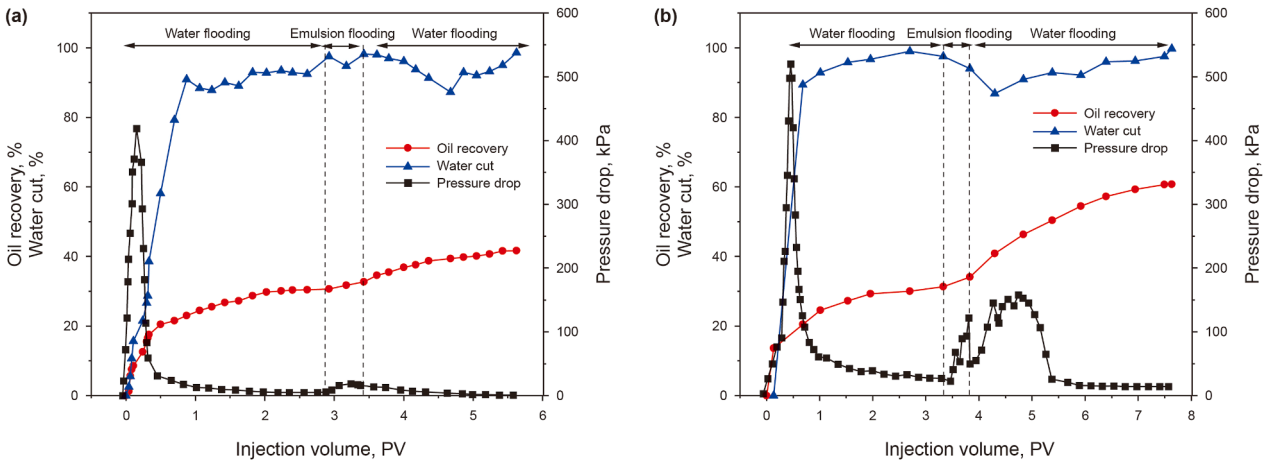

Fig. 11. Comparative single-core flooding performance. (**a**) Surfactant-stabilized emulsion flooding (0.5 wt% LAO); (**b**) Pickering emulsion flooding (0.05 wt% LAO + 1.0 wt% nano-SiO_2).

Table 3
Summary of dual-core flooding experiments.

Permeability contrast	Core	Permeability, mD	Porosity, %	Initial oil saturation, %	Waterflooding oil recovery, %	Tertiary oil recovery, %	Cumulative oil recovery, %
3:1	Low-permeability	987	31.5	75.5	16.9	33.9	50.8
	High-permeability	2762	32.0	72.6	33.7	25.3	59.0
	Total				25.3	29.8	55.1
5:1	Low permeability	1071	30.4	72.4	9.5	46.2	55.7
	High permeability	5538	34.1	73.5	34.4	22.7	57.1
	Total				22.8	33.6	56.4

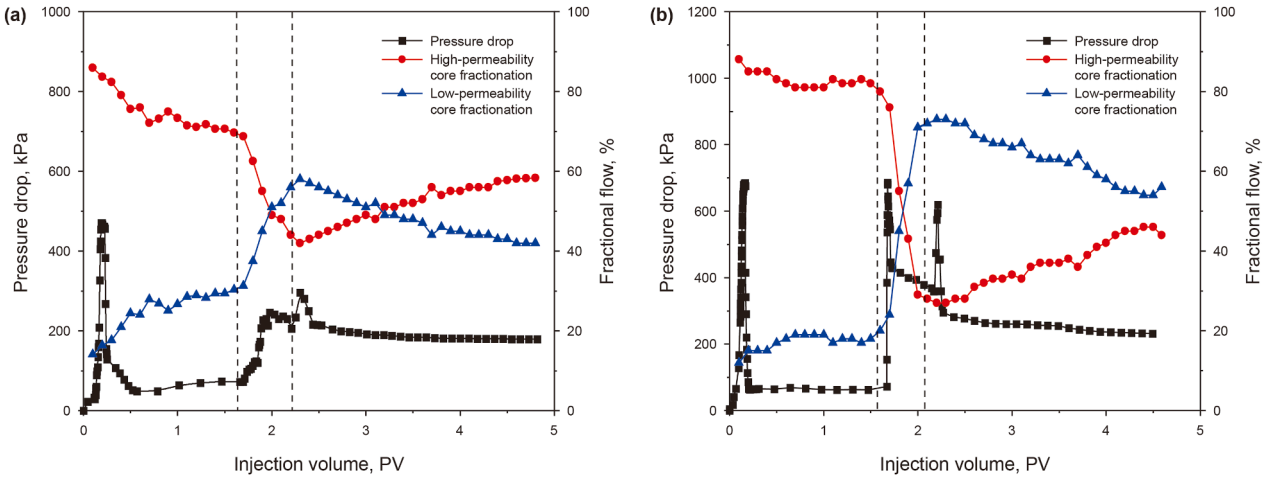

Fig. 12. Pressure drops and fractional flow curves of dual-core flooding with permeability contrasts of 3:1 (**a**) and 5:1 (**b**).

highly mobile, low-viscosity mixtures (Fig. 13(c) and (d)) with enhanced flowability. This viscosity reduction significantly improved heavy oil mobility, leading to an improvement in displacement efficiency. The synergistic combination of nanoparticle stabilization and aromatic hydrocarbon solvation established optimal conditions for heavy oil viscosity reduction, representing a critical mechanism in the enhanced heavy oil recovery process (Pei et al., 2024).

Microscopic analysis revealed significant residual heavy oil retention within pore spaces following initial waterflooding (Fig. 14(a)). The introduction of Pickering emulsions promoted the emulsification of this trapped oil through synergistic surfactant-nanoparticle interactions, where LAO-modified SiO_2 nanoparticles and surfactant collaboratively emulsified aggregated residual oil into mobile oil-in-water (O/W) emulsions (Fig. 14(b)). These emulsions exhibited a distinctive red-to-yellow transition under dynamic flow conditions (Fig. 14(c)), indicating successful oil mobilization. The emulsification process occurred through three synergistic mechanisms: (1) surfactant-mediated interfacial tension reduction facilitating oil droplet dispersion, (2) LAO-modified nano-SiO_2 stabilization preventing coalescence, and (3) flow-induced shear dispersion promoting droplet breakup and transport (Feng et al., 2018; Yue et al., 2022). The resulting O/W emulsion droplets efficiently migrated through complex pore networks (Fig. 14(d)), demonstrating effective mobilization of trapped oil. This process demonstrates the synergistic nanoparticle-surfactant interaction in mobilizing residual oil through emulsification, thus improving heavy oil displacement efficiency.

3.5.2. Flow diversion via Jamin-effect pore-throat blockage

Microscopic studies identified two distinct pore-scale flow diversion mechanisms facilitated by nanoparticle-stabilized Pickering emulsions and heavy oil-in-water (O/W) emulsions through sustained Jamin effects. Micromodel flooding experiments within a bimodal pore network (with average diameters of 60 μm for macropores and 10 μm for micropores) demonstrated that Pickering emulsion droplets (1–10 μm) initiate Jamin-effect blockage primarily via selective accumulation at pore throats, particularly within macropores. Although most droplets were smaller than macropore throats (> 10 μm), hydrodynamic focusing and interfacial interactions promoted their aggregation into transient clusters at these constrictions (Fig. 15(a) and (b)). Crucially, the high elastic modulus of the nanoparticle-stabilized interfacial layer prevented droplet coalescence, enabling these aggregates to form persistent, jammed structures that were stable under elevated flow pressures (Guillen et al., 2012). These robust blockages effectively redirect subsequent fluid flow into adjacent pore networks, including unblocked macropore regions and micropores (Fig. 15(c) and (d)). This process significantly altered preferential flow paths, substantially improving macroscopic sweep efficiency.

A secondary mechanism occurred during heavy oil mobilization, where the nanoparticle-surfactant system generated stable O/W emulsions. As shown in Fig. 16, these droplets could exceed micropore throat dimensions. When approaching pore-throat sizes, capillary trapping induced a pronounced Jamin effect, increasing flow resistance and enhancing fluid diversion. These dual mechanisms operated synergistically across the pore-size distribution: nanoparticle-stabilized Pickering emulsions

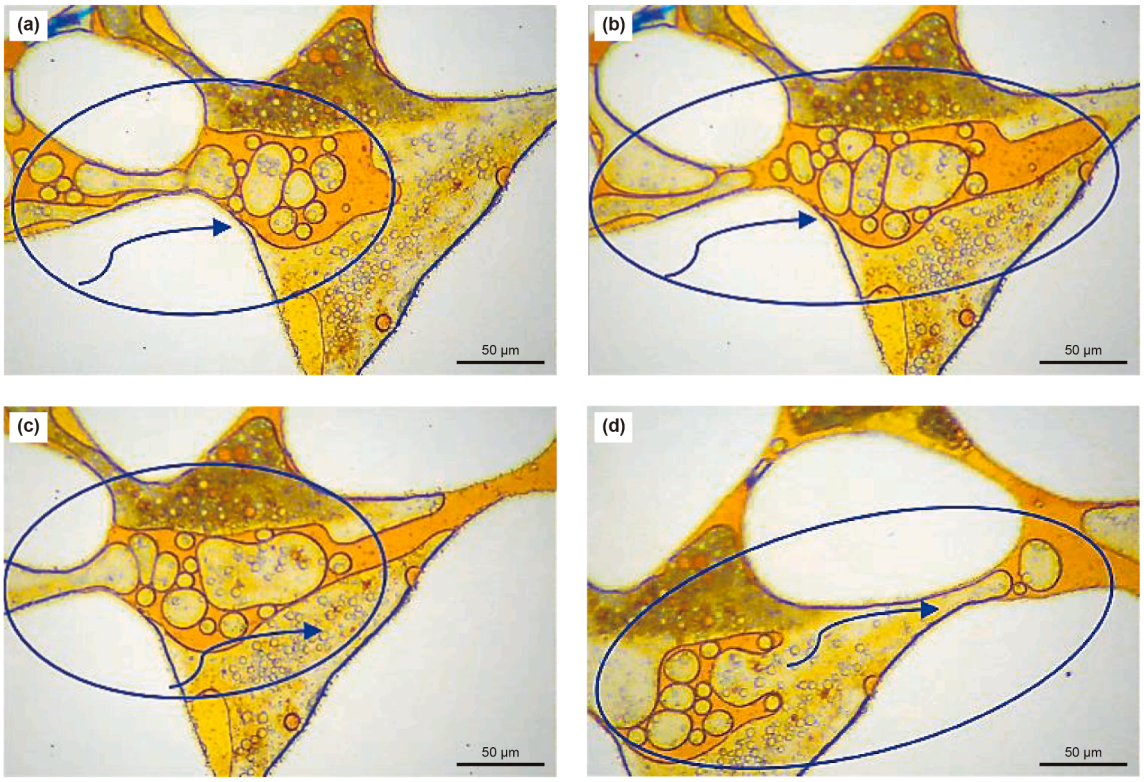

Fig. 13. Microscopic visualization of viscosity reduction for enhanced heavy oil mobility. (**a**) Initial emulsion–oil contact and droplet penetration; (**b**) viscosity reduction front (red to yellow transition); (**c**) formation of mobile mixture; (**d**) flow-enhanced heavy oil mobilization.

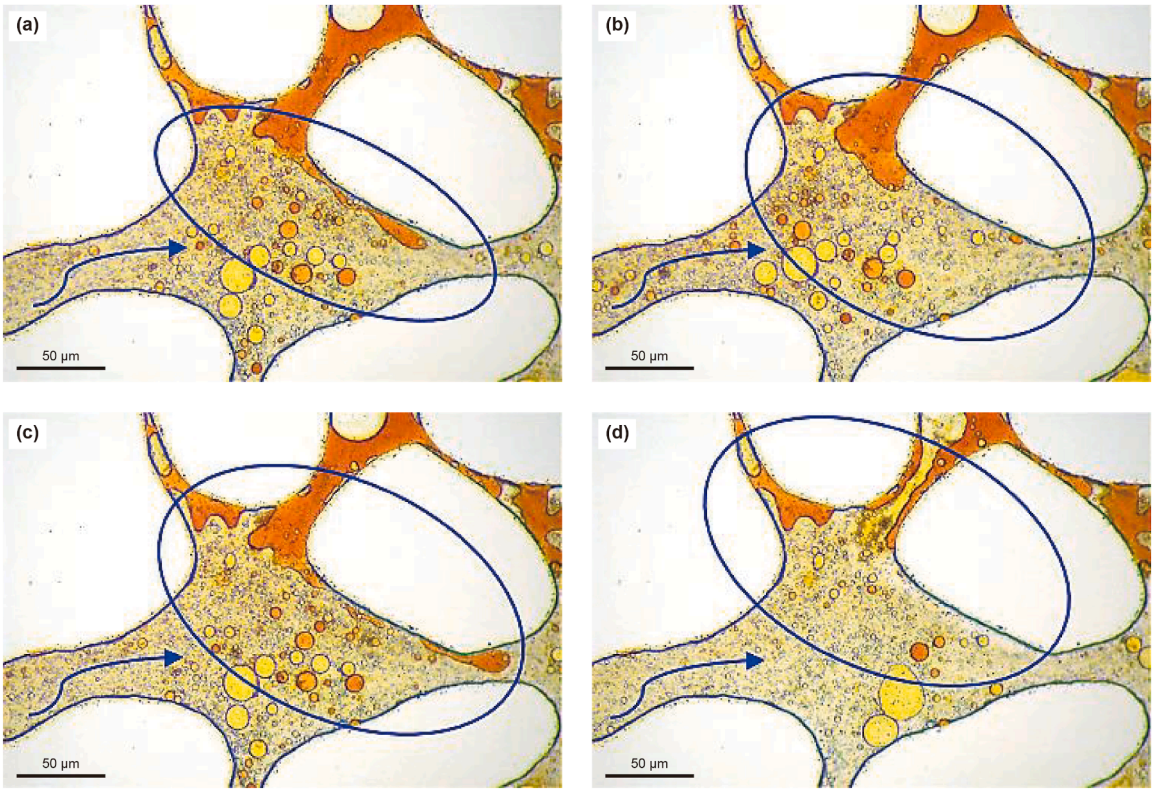

Fig. 14. Microscopic visualization of emulsification for enhanced heavy oil mobility. (**a**) Trapped oil clusters after waterflooding; (**b**) interfacial instability and droplet generation; (**c**) formed mobile O/W emulsions; (**d**) O/W emulsion migration through pore networks.

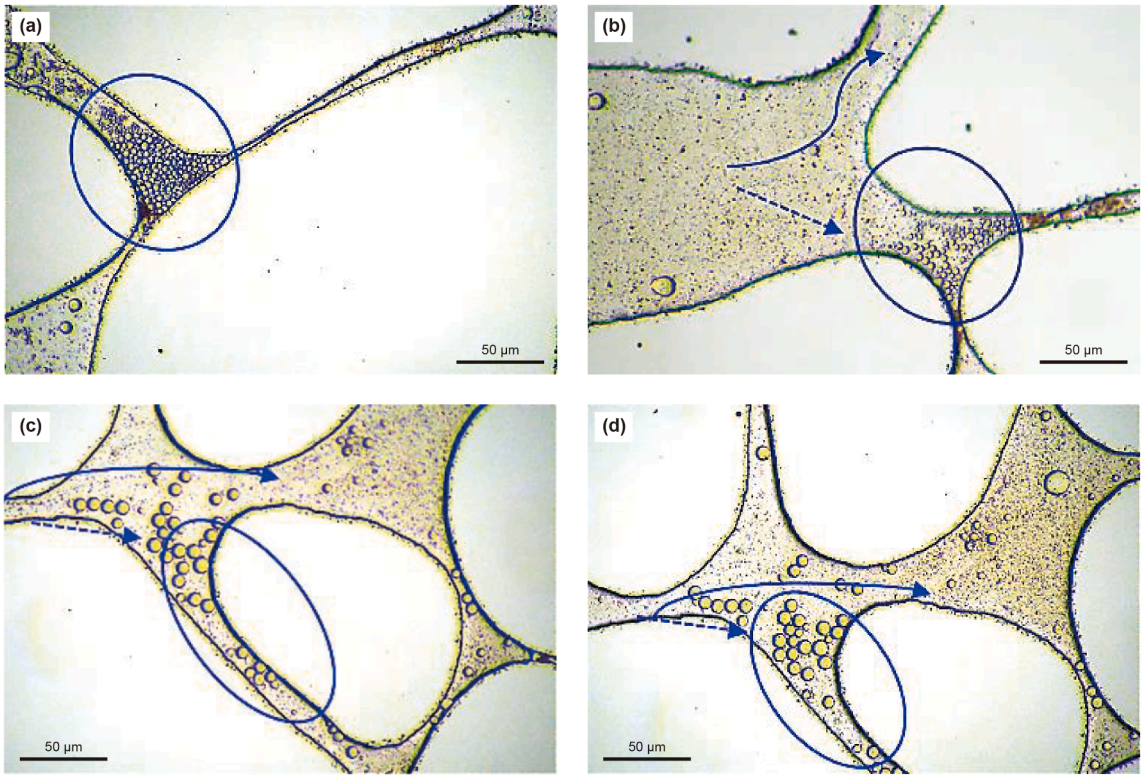

Fig. 15. Microscopic visualization of flow diversion via pore-throat blockage mechanisms. (**a**, **b**) Selective accumulation and jamming of Pickering emulsion droplets; (**c**, **d**) flow diversion into unblocked macropores and micropores.

dominated flow control in macroporous regions through jamming-induced blockage, while capillary-trapped O/W emulsion droplets regulated flow in constricted micropore throats (de Amorim et al., 2023; Liu et al., 2019). Their complementary interaction created a hierarchical, multiscale diversion system, significantly enhancing conformance control and volumetric sweep efficiency.

3.5.3. *Pore-scale viscoelastic mobilization of residual oil*

Conventional waterflooding faces inherent limitations in oil recovery efficiency, primarily resulting from viscous fingering and poor sweep efficiency. These shortcomings lead to substantial residual oil retention, manifested in three characteristic morphological configurations within porous media: (1) isolated oil blocks, (2) discontinuous oil clusters, and (3) pore-wall-adhered oil films. These morphologies represent the primary trapping mechanisms after conventional waterflooding. Nanoparticle-stabilized Pickering emulsions overcome these limitations through their distinct viscoelastic properties. Their elastic-dominated rheological behavior ($G' > 10G''$) enables the effective deformation and mobilization of trapped oil phases that are unrecoverable by conventional waterflooding. The viscoelastic modulus is a fundamental parameter controlling oil mobilization capacity and displacement efficiency. Fig. 17 presents microscopic visualization of the viscoelastic mobilization mechanisms for these residual oil morphologies.

(I) Dislodgment and extrusion of pore-throat trapped oil blocks

The viscoelastic Pickering emulsions mobilize a trapped oil block through a two-stage mechanism. As shown in Fig. 17(a1), the rigid, nanoparticle-stabilized interface first generates sufficient

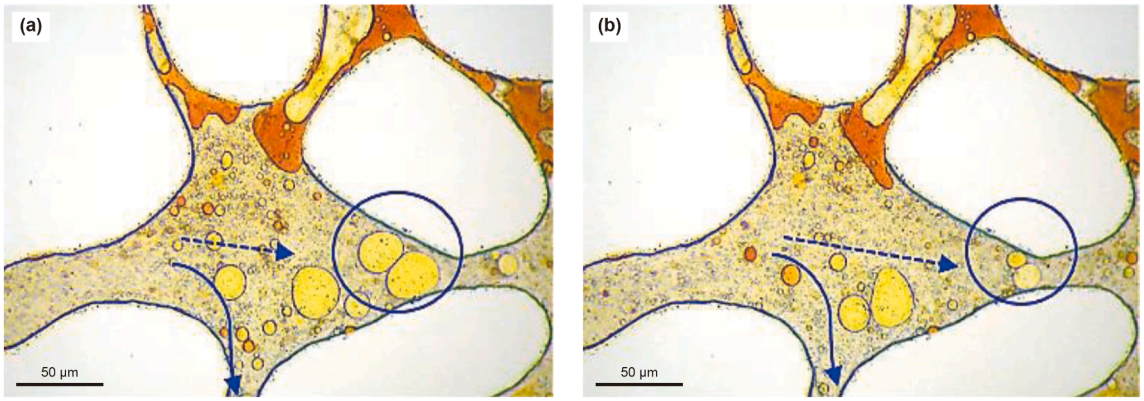

Fig. 16. Microscopic visualization of Jamin-effect-induced blockage by O/W emulsion droplets.

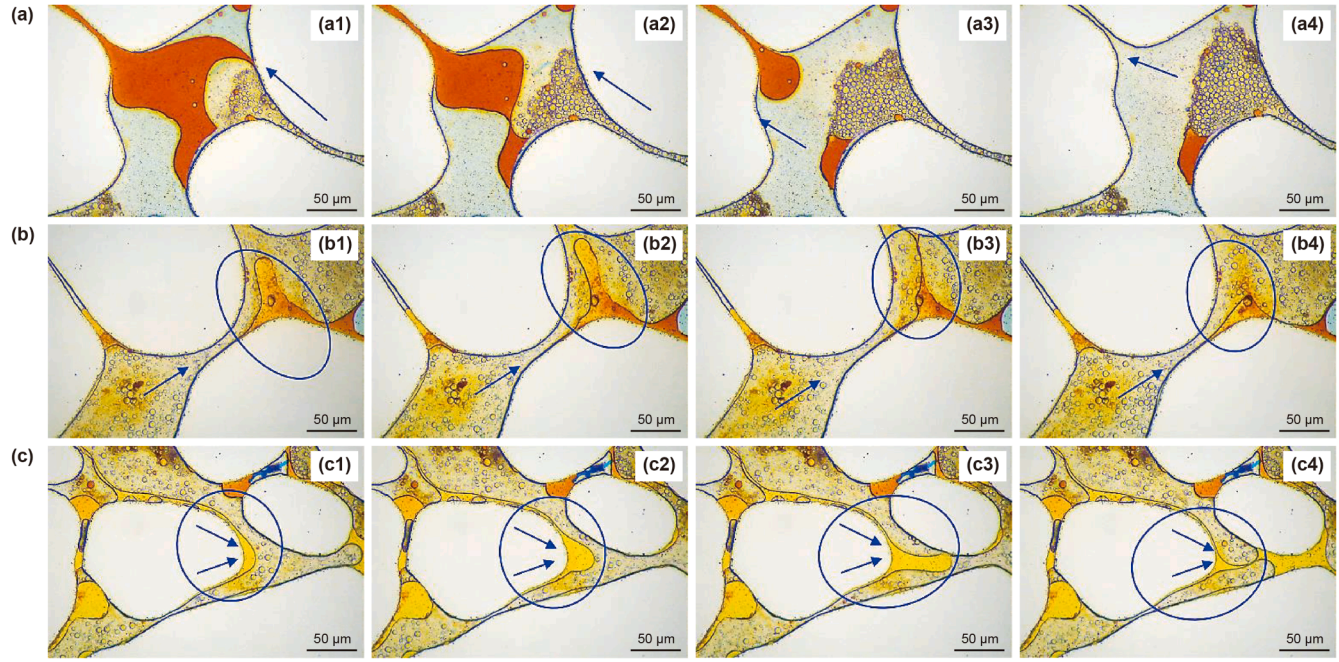

Fig. 17. Microscopic visualization of viscoelastic mobilizations for three residual oil morphologies. (**a**) Dislodgement and extrusion of oil blocks in pore throats; (**b**) viscoelastic deformation and mobilization of oil clusters; (**c**) interfacial roll-up and detachment of adhered oil films.

force to dislodge the oil block from the pore wall. Subsequently, a continuous flow of emulsion droplets induces progressive compression (Fig. 17(a2)), functioning as a piston-like displacement to extrude the oil block through the pore throat. This process causes the ganglion to progressively deform and elongate (Fig. 17 (a3)), ultimately leading to its complete detachment (Fig. 17(a4)). This unique viscoelastic behavior enables the mobilization of oil blocks resistant to waterflooding by providing the required mechanical driving force.

(II) Viscoelastic deformation and mobilization of oil clusters

The viscoelastic Pickering emulsions mobilize trapped oil clusters through a synergistic dual mechanism. As demonstrated in Fig. 17(b1), the emulsion's high-storage-modulus interface first generates compressive stresses, which induce structural deformation and elongation of the immobilized oil cluster (Fig. 17(b2)). Subsequently, shear-induced fragmentation occurs as the flowing emulsion progressively stretches and disaggregates the cluster into smaller, mobile droplets (Fig. 17(b3) and (b4)). This combined viscoelastic stress field proves more effective than the purely viscous drag forces of conventional flooding methods, enabling the emulsion to overcome capillary resistance and enhance microscopic displacement efficiency.

(III) Interfacial roll-up and detachment of adhered oil films

The viscoelastic Pickering emulsions mobilize oil films adhered to pore walls through a progressive three-stage mechanism, as shown in Fig. 17(c). First, the elastic, nanoparticle-laden interface acts as a mechanical displacer, initiating the roll-up of the oil film upon contact (Fig. 17(c1)). Subsequently, the thin oil film transforms into a spherical blob through interfacial coalescence (Fig. 17 (c2)). Finally, the stored elastic energy of the interface synergizes with hydrodynamic shear forces to facilitate the detachment and elongation of the droplet (Fig. 17(c3) and (c4)). This distinctive viscoelastic extrusion mechanism proves particularly effective for recovering strongly adhered residual oil films that are resistant to conventional flooding methods.

The three complementary mechanisms operate synergistically to enhance oil recovery by effectively targeting the full spectrum of pore-scale residual oil morphologies. This Pickering emulsion system is particular effective due to its nanoparticle-stabilized interface, which generates precisely tuned viscoelastic stresses (Lee and Babadagli, 2022). The system delivers compressive-dominated stresses to overcome capillary trapping of oil blocks and clusters, facilitating their physical extrusion from pore throats. Simultaneously, it produces shear-dominated stresses that promote the roll-up and detachment of thin oil films from pore walls. By employing this comprehensive force spectrum, the system ensures the complete mobilization of residual oil in heterogeneous pore networks, resulting in significant improvements in both microscopic displacement efficiency and overall recovery.

4. Conclusions

This study successfully developed and characterized a high-performance Pickering emulsion stabilized by LAO-modified SiO_2 nanoparticles for enhanced heavy oil recovery in heterogeneous reservoirs. Through systematic optimization, an optimal formulation was established: 1.0 wt% nano-SiO_2 modified with 0.05 wt% LAO at pH 7.0, using 5 wt% aromatic solvent as the oil phase. Comprehensive experimental analysis revealed three key findings:

(1) The optimized emulsion exhibited exceptional stability (TSI < 5) with uniform droplet distributions (1–10 μm) and superior viscoelastic properties (G'/G'' > 10), maintaining > 90% viscosity recovery after shear deformation. These characteristics arise from the mechanically robust interfacial film formed by LAO-modified nanoparticles at the oil-water interface.
(2) Core flooding tests demonstrated outstanding performance in both homogeneous and heterogeneous porous media. The emulsion showed remarkable plugging capability

(F_R = 124.3, F_{RR} = 24.1) and achieved an incremental oil recovery of 29.6%, substantially exceeding conventional surfactant-stabilized emulsions (11.1%). Notably, in a system with a permeability contrast of 5:1, the emulsion maintained excellent conformance control while achieving 33.6% tertiary oil recovery.

(3) Microscopic visualization studies identified three synergistic recovery mechanisms: (i) viscosity reduction and emulsification for enhanced heavy oil mobility, (ii) flow diversion induced by the Jamin effect at pore throats, and (iii) pore-scale viscoelastic mobilization of residual oil. These mechanisms collectively enhance both macroscopic sweep efficiency and microscopic displacement efficiency.

These findings provide fundamental insights for designing nanoparticle-stabilized Pickering emulsion for enhanced oil recovery. The demonstrated efficacy highlights the potential of LAO-modified nano-SiO_2-stabilized Pickering emulsion as a technologically viable solution for heavy oil recovery in heterogeneous reservoirs, effectively addressing critical challenges in emulsion stability, mobility control, and recovery efficiency.

CRediT authorship contribution statement

Hai-Hua Pei: Writing – review & editing, Funding acquisition, Conceptualization. **Jian-Wei Zhao:** Writing – original draft, Methodology, Investigation. **Yang Liu:** Investigation, Formal analysis, Data curation. **Jian Zhang:** Investigation, Formal analysis, Data curation. **Gui-Cai Zhang:** Validation, Supervision.

Declaration of interests

The authors declare that they have no known competing financial interests or personal relationships that could have appeared to influence the work reported in this paper.

Acknowledgements

The authors acknowledge the financial support of the National Key Research and Development Program of China (2018YFA0702400) and the Shandong Provincial Natural Science Foundation (ZR2019 MEE085).

References

Adil, M., Onaizi, S.A., 2022. Pickering nanoemulsions and their mechanisms in enhancing oil recovery: A comprehensive review. Fuel 319, 123667. https://doi.org/10.1016/j.fuel.2022.123667.

Ahmadi, M., Chen, Z.X., 2020. Challenges and future of chemical assisted heavy oil recovery processes. Adv. Colloid Interface Sci. 275, 102081. https://doi.org/10.1016/j.cis.2019.102081.

Ahmadi, P., Asaadian, H., Kord, S., Khadivi, A., 2019. Investigation of the simultaneous chemicals influences to promote oil-in-water emulsions stability during enhanced oil recovery applications. J. Mol. Liq. 275, 57–70. https://doi.org/10.1016/j.molliq.2018.11.004.

Benyaya, M., Bolzinger, M.A., Chevalier, Y., Bordes, C., 2024. Rheological properties and stability of Pickering emulsions stabilized with differently charged particles. Colloids Surf. A Physicochem. Eng. Asp. 687, 133514. https://doi.org/10.1016/j.colsurfa.2024.133514.

Binks, B.P., Desforges, A., Duff, D.G., 2007. Synergistic stabilization of emulsions by a mixture of surface-active nanoparticle and surfactant. Langmuir 23 (3), 1098–1106. https://doi.org/10.1021/la062510y.

Chen, K., Chen, M., Feng, Y., Yu, G., Zhang, L., Li, J., 2017. Application and rheology of anisotropic particle stabilized emulsions: Effects of particle hydrophobicity and fractal structure. Colloids Surf. A Physicochem. Eng. Asp. 524, 8–16. https://doi.org/10.1016/j.colsurfa.2017.02.088.

Chevalier, Y., Bolzinger, M.A., 2013. Emulsions stabilized with solid nanoparticles: Pickering emulsions. Colloids Surf. A Physicochem. Eng. Asp. 439, 23–34. https://doi.org/10.1016/j.colsurfa.2013.02.054.

de Amorim, C., de Almeida, R.V., Ponce, R.V., Carvalho, M.S., 2023. Visualization and quantification of mobility reduction in porous media flow associated with pore blocking by emulsion drops. Ind. Eng. Chem. Res. 62 (51), 22093–22102. https://doi.org/10.1021/acs.iecr.3c03340.

Demikhova, I.I., Likhanova, N.V., Perez, J.R.H., Falcon, D.A.L., Olivares-Xometl, O., Berthier, A.E.M., Lijanova, I.V., 2016. Emulsion flooding for enhanced oil recovery: Filtration model and numerical simulation. J. Petrol. Sci. Eng. 143, 235–244. https://doi.org/10.1016/j.petrol.2016.02.018.

Ding, B.X., Dong, M.Z., Chen, Z.X., Kantzas, A., 2022. Enhanced oil recovery by emulsion injection in heterogeneous heavy oil reservoirs: Experiments, modeling and reservoir simulation. J. Petrol. Sci. Eng. 209, 109882. https://doi.org/10.1016/j.petrol.2021.109882.

Dong, X.H., Liu, H.Q., Chen, Z.X., Wu, K.L., Lu, N., Zhang, Q.C., 2019. Enhanced oil recovery techniques for heavy oil and oilsands reservoirs after steam injection. Appl. Energy 239, 1190–1211. https://doi.org/10.1016/j.apenergy.2019.01.244.

Duodu, E.K., Ju, B.S., 2025. Cutting-edge research on nanoparticles used in unconventional oil development: A comprehensive review. Phys. Fluids 37 (3), 031303. https://doi.org/10.1063/5.0255639.

Feng, H., Kang, W., Zhang, L., Chen, J., Li, Z., Zhou, Q., Wu, H.R., 2018. Experimental study on a fine emulsion flooding system to enhance oil recovery for low permeability reservoirs. J. Petrol. Sci. Eng. 171, 974–981. https://doi.org/10.1016/j.petrol.2018.08.011.

Fuma, T., Kawaguchi, M., 2015. Rheological responses of Pickering emulsions prepared using colloidal hydrophilic silica particles in the presence of NaCl. Colloids Surf. A Physicochem. Eng. Asp. 465, 168–174. https://doi.org/10.1016/j.colsurfa.2014.10.050.

Gomaa, S., Salem, K.G., El-hoshoudy, A.N., 2024. Enhanced heavy and extra heavy oil recovery: Current status and new trends. Petroleum 10 (3), 399–410. https://doi.org/10.1016/j.petlm.2023.10.001.

Guillen, V.R., Carvalho, M.S., Alvarado, V., 2012. Pore scale and macroscopic displacement mechanisms in emulsion flooding. Transport Porous Media 94, 197–206. https://doi.org/10.1007/s11242-012-9997-9.

Heidari-Dalfard, F., Tavasoli, S., Assadpour, E., Miller, R., Jafari, S.M., 2024. Surface modification of particles/nanoparticles to improve the stability of Pickering emulsions: A critical review. Adv. Colloid Interface Sci. 336, 103378. https://doi.org/10.1016/j.cis.2024.103378.

Jia, H., Kang, Y.H., 2025. A comprehensive review on application and perspectives of nanomaterials in enhanced oil recovery. Energy & Fuels 39 (6), 2916–2942. https://doi.org/10.1021/acs.energyfuels.4c04848.

Kargozarfard, Z., Riazi, M., Ayatollahi, S., 2019. Viscous fingering and its effect on areal sweep efficiency during waterflooding: An experimental study. Pet. Sci. 16, 105–116. https://doi.org/10.1007/s12182-018-0258-6.

Karambeigi, M.S., Abbassi, R., Roayaei, M., Emadi, M.A., 2015. Emulsion flooding for enhanced oil recovery: Interactive optimization of phase behavior, microvisual and core-flood experiments. J. Ind. Eng. Chem. 29, 382–391. https://doi.org/10.1016/j.jiec.2015.04.019.

Kumar, G., Mani, E., Sangwai, J.S., 2023. Impact of surface-modified silica nanoparticle and surfactant on the stability and rheology of oil-in-water Pickering and surfactant-stabilized emulsions under high-pressure and high-temperature. J. Mol. Liq. 379, 121620. https://doi.org/10.1016/j.molliq.2023.121620.

Kumar, N., Mandal, A., 2018. Surfactant stabilized oil-in-water nanoemulsion: Stability, interfacial tension, and rheology study for enhanced oil recovery application. Energy & Fuels 32 (6), 6452–6466. https://doi.org/10.1021/acs.energyfuels.8b00043.

Lee, J., Babadagli, T., 2022. Optimal design of Pickering emulsions for heavy-oil recovery improvement. J. Dispersion Sci. Technol. 41 (13), 2048–2062. https://doi.org/10.1080/01932691.2019.1650754.

Li, H.F., Wang, Q., Wu, Y.B., 2023. Current status and development direction of low-carbon exploitation technology for heavy oil. Energies 16 (5), 2219. https://doi.org/10.3390/en16052219.

Li, K., Ovsepian, M., Xie, W., Varfolomeev, M.A., Luo, Q., Yuan, C., 2024. Emulsions for enhanced oil recovery: Progress and prospect. J. Mol. Liq. 393, 123658. https://doi.org/10.1016/j.molliq.2023.123658.

Liang, T., Hou, J.R., Qu, M., Xi, J.X., Raj, I., 2022. Application of nanomaterial for enhanced oil recovery. Pet. Sci. 19 (2), 882–899. https://doi.org/10.1016/j.petsci.2021.11.011.

Liu, J.X., Zhu, H.J., Pan, W., Pan, J.M., 2021. Recent studies of Pickering emulsion system in petroleum treatment: The role of particles. Pet. Sci. 18, 1551–1563. https://doi.org/10.1016/j.petsci.2021.10.001.

Liu, Z., Li, Y., Luan, H., Gao, W., Guo, Y., Chen, Y., 2019. Pore scale and macroscopic visual displacement of oil-in-water emulsions for enhanced oil recovery. Chem. Eng. Sci. 197, 404–414. https://doi.org/10.1016/j.ces.2019.01.001.

Liu, Z.X., Liang, Y., Wang, Q., Guo, Y.J., Gao, M., Wang, Z.B., 2020. Status and progress of worldwide EOR field applications. J. Petrol. Sci. Eng. 193, 107449. https://doi.org/10.1016/j.petrol.2020.107449.

Mahboob, A., Kalam, S., Kamal, M.S., Hussain, S.S., Solling, T., 2022. EOR perspective of microemulsions: A review. J. Petrol. Sci. Eng. 208, 109312. https://doi.org/10.1016/j.petrol.2021.109312.

Malozyomov, B.V., Martyushev, N.V., Kukartsev, V.V., Tynchenko, V.S., Bukhtoyarov, V.V., Wu, X., Tynchenko, Y.A., Kukartsev, V.A., 2023. Overview of methods for enhanced oil recovery from conventional and unconventional reservoirs. Energies 16 (13), 4907. https://doi.org/10.3390/en16134907.

Mariyate, J., Bera, A., 2021. Recent progresses of microemulsions-based nanofluids as a potential tool for enhanced oil recovery. Fuel 306, 121640. https://doi.org/10.1016/j.fuel.2021.121640.

Mariyate, J., Bera, A., 2022. A critical review on selection of microemulsions or nanoemulsions for enhanced oil recovery. J. Mol. Liq. 353, 118791. https://doi.org/10.1016/j.molliq.2022.118791.

Maurya, N.K., Mandal, A., 2018. Investigation of synergistic effect of nanoparticle and surfactant in macro emulsion based EOR application in oil reservoirs. Chem. Eng. Res. Des. 132, 370–384. https://doi.org/10.1016/j.cherd.2018.01.049.

Moradi, M., Kazempour, M., French, J.T., Alvarado, V., 2014. Dynamic flow response of crude oil-in-water emulsion during flow through porous media. Fuel 135, 38–45. https://doi.org/10.1016/j.fuel.2014.06.025.

Nourafkan, E., Gardy, J., Asachi, M., Ahmed, W., Wen, D., 2019. Nanoparticle formation in stable microemulsions for enhanced oil recovery application. Ind. Eng. Chem. Res. 58 (28), 12664–12677. https://doi.org/10.1021/acs.iecr.9b00760.

Pei, H.H., Shu, Z., Zhang, G.C., Ge, J.J., Jiang, P., Qin, Y., Cao, X., 2018. Experimental study of nanoparticle and surfactant stabilized emulsion flooding to enhance heavy oil recovery. J. Petrol. Sci. Eng. 163, 476–483. https://doi.org/10.1016/j.petrol.2018.01.025.

Pei, H.H., Zhao, J.W., Wu, Y.H., Liu, Y., Ning, C., Zhang, J., Zhang, G.C., 2024. Synergistic stabilization of emulsified solvent by nanobentonite and alkylethoxyglucoside to improve heavy oil recovery. Energy & Fuels 38 (13), 11616–11626. https://doi.org/10.1021/acs.energyfuels.4c01936.

Qin, T.Z., Goual, L., Piri, M., Hu, Z.L., Wen, D.S., 2020. Nanoparticle-stabilized microemulsions for enhanced oil recovery from heterogeneous rocks. Fuel 274, 117830. https://doi.org/10.1016/j.fuel.2020.117830.

Salehnia, T., Parsaei, R., Riazi, M., Kazemzadeh, Y., 2025. An insight into the effect of surface-active agents on the interfacial viscosity and stability of oil-in-water emulsions. J. Mol. Liq. 426, 127370. https://doi.org/10.1016/j.molliq.2025.127370.

Santos, L.B.L., Silva, A.C.M., Pereira, K.R.O., Moraes, C., Gomes, A.L., Santos, J.P.L., Santos, L.C., 2023. Microemulsions stabilized with nanoparticles for EOR: A review. J. Mol. Liq. 391, 123271. https://doi.org/10.1016/j.molliq.2023.123271.

Sarma, H.K., Maini, B.B., Jha, K., 1998. Evaluation of emulsified solvent flooding for heavy oil recovery. J. Can. Pet. Technol. 37, 55–62. https://doi.org/10.2118/98-07-06.

Seidy-Esfahlan, M., Tabatabaei-Nezhad, S.A., Khodapanah, E., 2024. Comprehensive review of enhanced oil recovery strategies for heavy oil and bitumen reservoirs in various countries: Global perspectives, challenges, and solutions. Heliyon 10 (18), e37826. https://doi.org/10.1016/j.heliyon.2024.e37826.

Singh, P.K., Joshi, D., Mandal, A., Pal, N., 2025. Silica Nanoparticle-stabilized anionic surfactant microemulsions: Characterization, technical evaluation, and core-flooding studies for enhanced oil recovery. Energy & Fuels 39 (4), 1870–1888. https://doi.org/10.1021/acs.energyfuels.4c05091.

Su, H., Zhou, F.J., Liu, Y., Gao, Y.J., Cheng, B.Y., Dong, R.C., Liang, T.B., Li, J.J., 2021. Pore-scale investigation on occurrence characteristics and conformance control mechanisms of emulsion in porous media. Petrol. Explor. Dev. 48 (6), 1241–1249. https://doi.org/10.1016/S1876-3804(21)60299-9.

Sun, H.Q., Wang, H.T., Cao, X.L., Shu, Q.L., Fan, Z.Y., Wu, G.H., Yang, Y.L., Wu, Y.C., 2024. Innovations and applications of the thermal recovery techniques for heavy oil. Energy Geosci. 5 (4), 100332. https://doi.org/10.1016/j.engeos.2024.100332.

Wang, C., Liu, Y., Du, Y., Gao, Y., Sun, Y., 2021. Heavy-oil recovery by combined geothermal energy and cosolvent/water flooding. Energy 228, 120681. https://doi.org/10.1016/j.energy.2021.120681.

Worthen, A.J., Foster, L.M., Dong, J., Bollinger, J.A., Peterman, A.H., Pastora, L.E., Bryant, S.L., Truskett, T.M., Bielawski, C.W., Johnston, K.P., 2014. Synergistic formation and stabilization of oil-in-water emulsions by a weakly interacting mixture of zwitterionic surfactant and silica nanoparticles. Langmuir 30 (4), 984–994. https://doi.org/10.1021/la404132p.

Yang, L., Ge, J.J., Wu, H., Li, X.Q., Li, J.D., Zhang, G.C., 2024. Study on the enhanced oil recovery properties of the Pickering emulsions for harsh reservoirs. ACS Omega 9 (49), 48427–48437. https://doi.org/10.1021/acsomega.4c06834.

Yao, Y., Sun, D.Q., Xu, J.H., Wang, B., Peng, G.H., Sun, B.M., 2023. Evaluation of enhanced oil recovery methods for mature Continental heavy oil fields in China based on geology, technology and sustainability criteria. Energy 278, 127962. https://doi.org/10.1016/j.energy.2023.127962.

Yu, F.W., Jiang, H.Q., Fan, Z., Xu, F., Su, H., Li, J.J., 2019. Formation and flow behaviors of *in situ* emulsions in heavy oil reservoirs. Energy & Fuels 33 (7), 5961–5970. https://doi.org/10.1021/acs.energyfuels.9b00154.

Yue, L., Pu, W.F., Zhao, T.H., Zhuang, J., Zhao, S., 2022. A high performance magnetically responsive Janus nano-emulsifier: Preparation, emulsification characteristics, interfacial rheology, and application in emulsion flooding. J. Petrol. Sci. Eng. 208, 109478. https://doi.org/10.1016/j.petrol.2021.109478.

Zhang, Y.M., Ren, X.F., Guo, S., Liu, X.F., Fang, Y., 2018. CO_2-switchable Pickering emulsion using functionalized silica nanoparticles decorated by amine oxide-based surfactants. ACS Sustain. Chem. Eng. 6, 2641–2650. https://doi.org/10.1021/acssuschemeng.7b04162.

Zhou, Y., Yin, D., Chen, W., Liu, B., Zhang, X., 2019. A comprehensive review of emulsion and its field application for enhanced oil recovery. Energy Sci. Eng. 7 (4), 1046–1058. https://doi.org/10.1002/ese3.354.